1.88 µm, Ba(NO₃)₂-based Raman laser pumped by a potassium-titanyl-phosphate-based optical parametric oscillator laser

Junchi Chen (陈俊驰)[1,2,3], **Xiao Zou** (邹 晓)[2,3], **Yujie Peng** (彭宇杰)[2,*],
Hongpeng Su (苏泓彭)[2,3], and **Yuxin Leng** (冷雨欣)[2,**]

¹*School of Physics Science and Engineering, Tongji University, Shanghai 200092, China*

²*State Key Laboratory of High Field Laser Physics, Shanghai Institute of Optics and Fine Mechanics,*
Chinese Academy of Sciences, Shanghai 201800, China

³*University of Chinese Academy of Science, Beijing 100190, China*

*Corresponding author: yjpeng@siom.ac.cn; **corresponding author: lengyuxin@mail.siom.ac.cn

Received May 16, 2016; accepted September 23, 2016; posted online October 26, 2016

A 1.88 µm Ba(NO₃)₂-based stimulated Raman scattering (SRS) laser pumped by a potassium-titanyl-phosphate-based optical parametric oscillator (OPO) laser is presented. Under the pumping energy of a 130 mJ 1064 nm *Q*-switched Nd:YAG laser, a 40 mJ 1.57 µm laser is achieved; the maximum output energy of the 1.88 µm Raman laser reaches 7.5 mJ with a pulse duration of 5.3 ns at repetition rates of 10 Hz, and the corresponding total optical conversion efficiency is about 5.8%. The combination of the SRS and OPO techniques significantly extends the wavelength from 1.064 to 1.57 µm (OPO) and then demonstrates Stokes-shifting to 1.88 µm (SRS).

OCIS codes: 140.3550, 140.3538, 190.5650, 190.4970.
doi: 10.3788/COL201614.111401.

The 1.88 µm lasers have many potential applications, since absorption optics bands of the water vapor are located near 0.94, 1.13, 1.38, and 1.88 µm. It has been demonstrated that both the 1.38 and 1.88 µm channels are highly sensitive in detecting the upper level cirrus clouds, and the 1.88 µm channel is more sensitive to changes in the ice particles' size distributions than the 1.38 µm channel[1]. Furthermore, it is an excellent pumping source for Ho-doped media with an absorption band of 1.86–1.93 µm. Presently, a few laser systems based on the Tm-doped media have successfully generated 1.88 µm radiation, since the fluorescence spectral band of the Tm-doped crystal from the ³F₄ energy level to the ³H₆ energy level covers from 1.6 to 2.2 µm, and 1.88 µm is located at the third emission peak[2–4]. However, most of these 1.88 µm lasers have low output energy and low peak power, and the Tm-doped media-based lasers are usually operated over 1.9 µm, owing to the reabsorption to the laser below 1.9 µm[5–7]. There are continuing efforts for either developing new techniques to produce 1.88 µm lasers or achieving frequency conversion of existing laser sources. Optical parametric oscillators (OPOs) and stimulated Raman scattering (SRS) are reliable and feasible techniques for realizing a frequency shift and generating diverse wavelengths.

An OPO is widely studied in terms of second-order nonlinear interaction, and it has been proved to be an efficient nonlinear frequency conversion method for obtaining various wavelengths from visible light to far-infrared. OPO laser systems have been demonstrated based on typical crystals, such as potassium titanyl arsenate (KTA), rubidium titanyl phosphate (RTP)[8,9], and the periodically poled crystal MgO:PPLN[10], as well as GaAs and zinc germanium phosphide (ZGP)[11,12] yielding lasers operating beyond 5 µm. Another excellent nonlinear crystal, potassium titanyl phosphate (KTP), which is known for its perfect nonlinear properties, has been established as one of the most important materials in OPOs, especially for obtaining lasers operating in the eye-safe wave band[13,14]. SRS in terms of third-order nonlinear processes has been proved to be an economical and practical technique for frequency conversion, pulse compression, and beam profile clean-up. Solid-state Raman lasers are particularly developed because the solid Raman media are characterized with high gain, high thermal efficiency, and high damage threshold compared with SRS lasers based on gas and liquid media. Thus far, continuous wave, femtosecond, picosecond, as well as nanosecond lasers, operating in the wavelength range from visible light to mid-infrared, have been demonstrated based on the solid Raman gain media[15–17]. One of the attractive Raman gain media refers to the Ba(NO₃)₂ crystal that maintains a large Raman shift (1047 cm⁻¹) and a large Raman gain (11 cm/GW at 1064 nm), which is widely used for SRS generation and amplification[18,19]. The combination of SRS and OPO techniques can considerably extend the obtainable spectral ranging. As reported in Ref. [20], a 1.81 µm OPO laser based on the KTP crystal was successfully achieved, and the pumping source was from an acoustic, optically *Q*-switched Nd:YAG/SrWO₄ intracavity Raman 1180 nm laser. Sabella *et al.* reported that continuously tunable mid-infrared Raman lasers operating from 3.38 to 3.8 µm with a pulse energy of about 80 µJ can be achieved based on diamond crystals pumped

by an idler signal laser from an OPO laser[21]. However, in most of these laser systems, the obtained output energy is below the order of millijoules, the peak intensity is below the order of megawatts, and there has been no report on achieving a 1.88 μm Raman laser output based on the system combining the SRS and OPO techniques.

In this Letter, a 1.88 μm Raman laser based on a $Ba(NO_3)_2$ crystal with energy up to 7.5 mJ at frequency rates of 10 Hz is successfully achieved through combining the external cavity OPO and SRS techniques. A 130 mJ, 1064 nm Q-switched Nd:YAG laser is delivered into the KTP-based OPO external cavity, and a 1.57 μm laser with an energy of 40 mJ is obtained. Then, the 1.57 μm laser is employed as the pumping source for the Raman laser based on the $Ba(NO_3)_2$ crystal, and 1.88 μm Raman laser with energy up to 7.5 mJ is successfully generally. The total optical conversion efficiency is about 5.8%. The measured energy fluctuation of the 1.88 μm is about 2.1% [root mean square (RMS)] within 600 s. The obtained pulse duration of the 1.88 μm laser is about 5.3 ns, which is lower than that of the original 1064 nm laser (7.7 ns), owing to compression during the OPO (pulse width of 6.2 ns) and SRS processes. Moreover, the maximum peak power can reach above 1.4 MW. The beam profiles of the 1064 nm, 1.57 μm, and 1.88 μm lasers are investigated here as well. The combination of the SRS and OPO is an effective way to generate a mid-infrared laser with a high peak intensity.

As presented in Fig. 1, the experimental setup is mainly composed of three parts, the initial 1064 nm pumping laser source, the KTP-based external cavity OPO, and the SRS laser based on the $Ba(NO_3)_2$ crystal. The 1064 nm pumping laser is a Q-switched Nd:YAG laser assembled in a commercial product (Quantel, CFR400). The 1064 nm laser can deliver a maximum energy of around 400 mJ with a pulse duration of 7.7 ns at the maximum repetition rates of 10 Hz. A half-wave plate (HWP) working together with the Faraday rotator (FR) is placed just after the Q-switched Nd:YAG laser to prevent unwanted back reflection of the pumping laser. The beam size of the multi-mode 1064 nm laser out of the source is about 7 mm, and the laser beam is then compressed by the following plane-convex lens L1 (focal length: 200 mm) and plane-concave lens L2 (focal length: −100 mm) before it is collimated into the OPO external cavity. The OPO laser only consists of a single KTP crystal of the size of
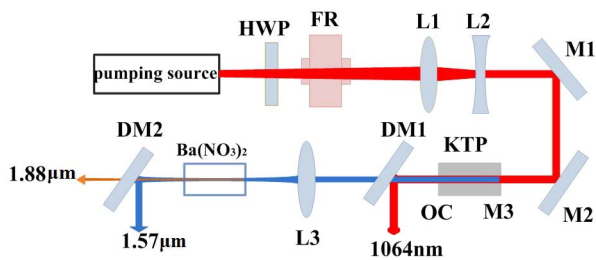
5 mm × 5 mm × 30 mm. The KTP crystal is cut for a type II noncritically phase-matched configuration to yield the maximum effective nonlinear coefficient and acceptance angle. The cavity mirrors are coated on the two ends of the KTP crystal, one end face, M3, is coated for antireflection at 1064 nm and high reflectivity at 1.57 μm, and the output coupler (OC) end face is coated for antireflection at 1064 nm and transmission efficiency of $T = 15\%$ at 1.57 μm. The cavity of the OPO laser coated on the two ends of the KTP crystal aims at obtaining a short optical path, although high machining precision is required. The short optical path allows the signal laser to be reflected as many times as possible to deplete the pumping laser energy during the pulse width time of the pumping laser. The dichroic mirrors (DM, high reflectivity at 1064 nm; antireflection at 1.57 μm) are located behind the OC in order to completely separate the 1.57 μm laser from the 1064 nm laser. Then, the 1.57 μm laser is focused by the lens with a focal length of 150 mm into the $Ba(NO_3)_2$ crystal of the size of 10 mm × 10 mm × 80 mm. No optical film is coated on the ends of the Raman crystal except for the SiO_2 film because the $Ba(NO_3)_2$ crystal is deliquescent. The DMs are located behind the $Ba(NO_3)_2$ crystal to separate the 1.88 μm laser from the 1.57 μm laser.

The spectra of the OPO and Raman lasers are first measured and presented in Fig. 2. The 1.57 μm signal wavelength of the OPO laser is in accordance with the noncritical phase matching, and the idler laser around 3.3 μm is not observed because it is strongly absorbed by the KTP crystal and barium borosilicate (BK7) mirrors. The detected wavelength of the first Stokes laser is 1.88 μm, which corresponds to the Stokes frequency shift of 1047 cm^{-1} of the $Ba(NO_3)_2$ crystal. Besides, the first-order anti-Stokes laser located at 1.35 μm is also observed with a very weak intensity, and hence, it can be neglected. The 1.35 μm anti-Stokes laser can be compressed through introducing an external cavity, which is composed of two cavity mirrors coated with antireflection at 1.35 μm.

The laser performances of the OPO and SRS lasers are shown in Fig. 3. The output energy of the 1.57 μm laser increases linearly as a function of the energy of the 1064 nm laser, as presented in Fig. 3(a). The maximum obtained energy of the 1.57 μm laser reaches 40 mJ under a pumping energy of 130 mJ at repetition rates of 10 Hz, corresponding to an optical conversion efficiency of 30.8%.

Fig. 1. Schematic layout of the $Ba(NO_3)_2$ SRS laser pumped by the KTP OPO laser.
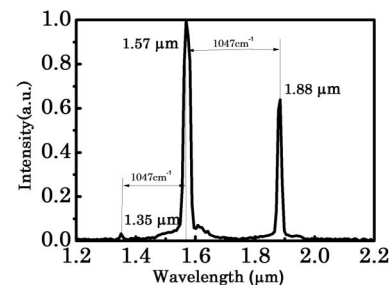
Fig. 2. Spectra of the monitored OPO and Raman lasers.
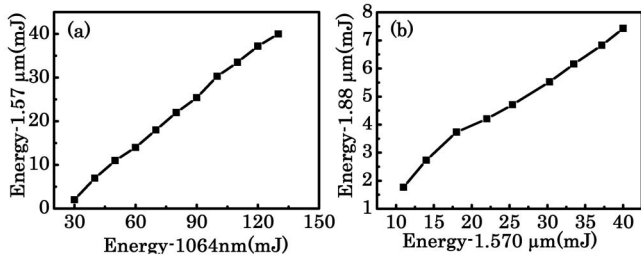
Fig. 3. (a) Output energy of the 1.57 μm laser in terms of the energy of the 1064 nm laser; (b) output energy of the 1.88 μm laser in terms of the energy of the 1.57 μm laser.

When the energy of the 1064 nm laser exceeds 150 mJ, unrecoverable optical damage to the ends of the KTP crystal and film coating occurs because of the inhomogeneous intensity distribution of the 1064 nm pumping laser. Therefore, the energy of the 1064 nm laser delivered to the OPO external cavity is limited to be below 130 mJ, and as a result, the output power and energy are limited. In fact, the output power and energy are mainly determined by the injected pumping laser energy. In order to achieve higher power and energy of the 1.57 μm laser, a KTP crystal with a larger dimension is needed to keep the pumping laser intensity below the threshold of optical damage to the crystal. The nonlinear frequency conversion efficiency and gain have relationships with the pumping laser intensity determined by the laser beam size when the pumping laser energy remains constant. The conversion can be largely improved by reducing the laser beam size under the condition that no optical damage happens. The output energy of the 1.88 μm laser in terms of the pumping energy of the 1.57 μm laser is depicted in Fig. 3(b). Under the maximum pumping energy of the 1.57 μm laser, a 7.5 mJ, 1.88 μm Raman laser is achieved. The optical conversion efficiency from the 1.57 μm laser to the 1.88 μm laser is about 18.8%, and the total optical efficiency of transforming the initial 1064 nm laser to the 1.88 μm Raman laser is about 5.8%. In fact, the absorption coefficient of the $Ba(NO_3)_2$ crystal becomes larger when the Raman laser exceeds 1.8 μm, thus the optical conversion efficiency is lower than the other $Ba(NO_3)_2$ crystal-based Raman laser. Furthermore, the optical conversion efficiency of the Raman laser is mainly determined by the pumping intensity, so the efficiency and energy can be considerably improved if the pumping energy of the 1.57 μm laser is also increased, which is work that needs further focus. It is also helpful to improve the optical conversion using the fundamental mode 1064 nm pumping laser instead of a non-homogeneous multi-mode one. The fundamental mode pumping laser can contribute to improving the intensity without causing damage to the KTP crystal. On the other hand, the conversion efficiency from the 1.57 μm laser to the 1.88 μm laser is also improved, accompanying the improved energy of the 1.57 μm laser. Additionally, the external cavity with a short cavity length adopted in the Raman laser system can contribute to improving the optical conversion efficiency of the

Raman laser. In fact, the output energy of the 1.88 μm laser can reach about 8.4 mJ, and the corresponding optical efficiency is raised to 21% if the L3 is replaced by a convex mirror with a focal length of 125 mm. However, the peak intensity of the 1.57 μm laser is close to the damage threshold of the $Ba(NO_3)_2$ crystal (400 MW/cm^2), so the L3 with a focal length of 150 mm is adopted in this system.

The main limitations for improving the optical conversion efficiency are the non-uniform intensity distributions of the original 1064 nm pumping laser and the damage threshold of the KTP crystal and coated film. Moreover, the absorption of the $Ba(NO_3)_2$ crystal to the 1.88 μm laser can affect the efficiency and output energy as well.

The output energy stabilities of the 1064 nm, 1.57 μm, and 1.88 μm lasers in terms of time is monitored operating up to 600 s and presented in Fig. 4. The energy fluctuation of the 1064 nm laser is 0.3% (RMS) in 600 s, as shown in Fig. 4(a), and the fluctuation of the 1.57 μm laser is about 0.56%, as shown in Fig. 4(b); the RMS value of the 1.88 μm laser output energy increases to 2.1%, as shown in Fig. 4(c). The main reason for the increased instability is due to the low energy of the 1.57 μm laser as a pumping source for the Raman laser, and the increasingly complicated system also influences the instability.

The temporal pulse shape of the 1064 nm laser, the OPO signal laser, and the first Stokes laser are monitored by an oscillograph (Tektronix, MDO3104) and photoelectric detector (Ultrafast, UPD-5N-IR2-P) and denoted by the black, blue, and red lines, respectively, in Fig. 5. The detected pulse durations of the OPO and SRS lasers are around 6.3 and 5.4 ns, as presented in Figs. 5(b) and 5(c), which are compressed compared with the pulse duration of 7.7 ns of the 1064 nm laser, since the front part of the pumping energy is depleted as the threshold energy. The achieved corresponding peak power of the 1.88 μm Raman laser can reach above 1.4 MW, which can also be adopted as a flexible pumping source for the OPO to extend the wavelength to a mid-infrared region.
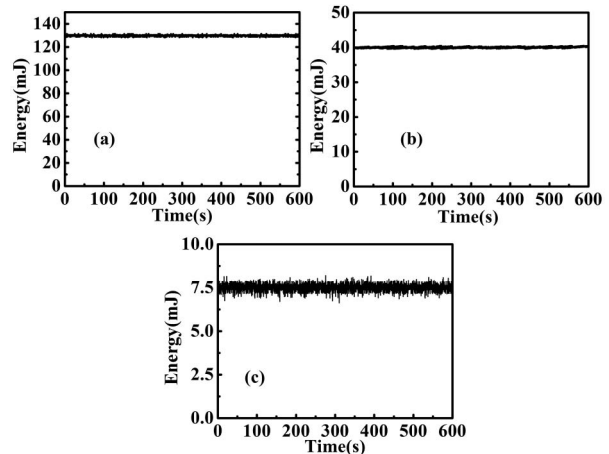
Fig. 4. Laser output energy stability in terms of time of up to 600 s. (a) Energy fluctuation of the 1064 nm laser versus time; (b) energy fluctuation of the 1.57 μm laser versus time; (c) energy fluctuation of the 1.88 μm laser versus time.
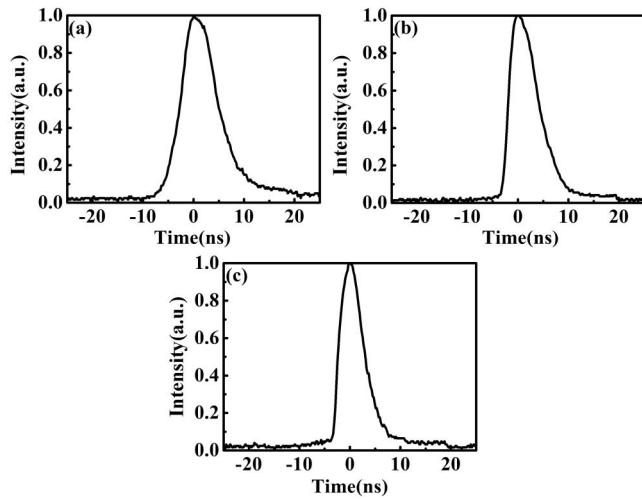
Fig. 5. Temporal pulse shape of lasers. (a) 1064 nm laser with a pulse width of 7.7 ns; (b) 1.57 µm laser with a pulse width of 6.3 ns; (c) 1.88 µm with a pulse width of 5.4 ns with the maximum output energy.
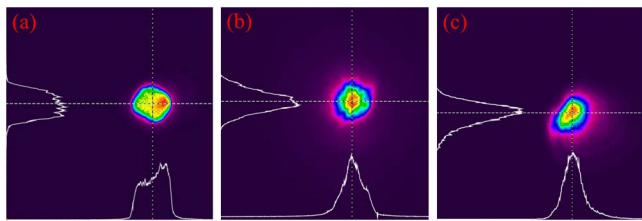
Fig. 6. Beam profiles of the lasers under the maximum SRS output energy. (a) 1064 nm; (b) 1.57 µm; (c) 1.88 µm.

The beam profiles of the 1064 nm, 1.57 µm, and 1.88 µm lasers in the far field are measured by a CCD and displayed in Figs. 6(a), 6(b), and 6(c), respectively. Because the Q-switched Nd:YAG laser is pumped by a single xenon lamp, the intensity distribution of the 1064 nm laser along the horizontal and vertical directions are non-homogeneous, as shown in Fig. 6(a). Moreover, the intensity distribution of the OPO laser is not smooth along these two directions as well. Although the beam profile of the first Stokes laser is asymmetrical, the intensity distribution becomes smooth along the horizontal and vertical directions owing to the beam clean-up effect during the SRS process. The beam qualities of the OPO laser and Raman laser denoted by factor β are 7.8 and 3.3, respectively, which suggest that the laser beam quality is improved through the SRS process.

The combination of the KTP-based OPO and $Ba(NO_3)_2$-based SRS frequency shifted techniques to obtain the 1.88 µm laser are demonstrated for the first time, to the best of our knowledge. The Raman laser is pumped by laser radiation from an external cavity OPO 1.57 µm laser, which employs a 1064 nm Q-switched Nd:YAG laser. The first Stokes 1.88 µm laser is obtained with an output energy of up to 7.5 mJ, operating at repetition rates of 10 Hz under 40 mJ. The 1.57 µm laser and the required energy of the 1064 nm laser is 130 mJ. The optical conversion

of the OPO converting wavelength from 1064 to 1.57 µm is about 30.8%, and the optical conversion of the SRS converting 1.57 to 1.88 µm is around 18.75%, yet the total optical conversion of the laser system is about 5.8%. The energy stabilities denoted by the RMS of the three lasers are also monitored to be 0.3%, 0.56%, and 2.1% with an operating time of up to 600 s. The measured pulse width of the 1.88 µm laser is approximately 5.3 ns, and this corresponding peak intensity is over 1.4 MW. The smoothness of the energy distribution of the 1.88 µm Raman laser is also improved. Our future work is to improve the operating frequency rate and output energy by adopting a 1064 nm pumping laser with a uniform intensity distribution and a KTP crystal against high intensity.

References

1. B. C. Gao, K. Meyer, and P. Yang, IEEE Trans. Geosci. Remote Sens. **42**, 1891 (2004).
2. S. Tessarin, M. Lynch, J. F. Donegan, and G. Maze, Electron. Lett. **41**, 899 (2005).
3. X. Liu, H. Huang, D. Shen, X. Liu, J. Zhang, and D. Tang, Chin. Opt. Let. **12**, 021404 (2014).
4. R. Faoro, M. Kadankov, D. Parisi, S. Veronesi, M. Tonelli, V. Petrov, U. Griebner, M. Segura, and X. Mateos, Opt. Let. **37**, 1517 (2012).
5. B. Yao, X. Li, H. Shi, T. Dai, Z. Cui, C. Qian, Y. Ju, and Y. Wang, Chin. Opt. Let. **13**, 101402 (2015).
6. C. Wang, S. Du, Y. Niu, Z. Wang, Q. Bian, C. Guo, J. Xu, Y. Bo, Q. Peng, D. Cui, and J. Zhang, Opt. Express **21**, 7156 (2013).
7. X. Zou, Y. Leng, Y. Li, Y. Feng, P. Zhang, Y. Hang, and J. Wang, Chin. Opt. Let. **13**, 081405 (2015).
8. H. Zhu, G. Zhang, H. Chen, C. Huang, W. Yong, Y. Duan, Y. Huang, H. Wang, and G. Qiu, Opt. Express **17**, 20669 (2009).
9. Y. Duan, H. Zhu, Y. Ye, D. Zhang, G. Zhang, and D. Tang, Opt. Let. **39**, 1314 (2014).
10. S. C. Kumar, J. Wei, J. Debray, V. Kemlin, B. Boulanger, H. Ishizuki, T. Taira, and M. Ebrahim-Zadeh, Opt. Let. **40**, 3897 (2015).
11. V. O. Smolski, S. Vasilyev, P. G. Schunemann, S. B. Mirov, and K. L. Vodopyanov, Opt. Let. **40**, 2906 (2015).
12. C. Kieleck, A. Berrou, B. Donelan, B. Cadier, T. Robin, and M. Eichhorn, Opt. Let. **40**, 1101 (2015).
13. C. Y. Cho, Y. C. Chen, Y. P. Huang, K. W. Su, and Y. F. Chen, Opt. Express **22**, 7625 (2014).
14. H. Chu, S. Zhao, K. Yang, J. Zhao, Y. Li, D. Li, G. Li, T. Li, and W. Qiao, Opt. Express **22**, 26925 (2014).
15. X. Li, Chin. Opt. Let. **14**, 021404 (2016).
16. M. Murtagh, J. Lin, R. P. Mildren, G. Mcconnell, and D. J. Spence, Opt. Express **23**, 15504 (2015).
17. V. I. Dashkevich, P. V. Shpak, S. V. Voitikov, R. V. Chulkov, A. S. Grabtchikov, E. A. Cheshev, M. Ei-Desouki, and V. A. Orhovich, Opt. Commun. **351**, 1 (2015).
18. X. Guo, J. Lu, W. Li, Y. Xu, X. Lu, Y. Leng, and R. Li, Opt. Laser Technol. **67**, 8 (2015).
19. N. Takei, S. Suzuki, and F. Kannari, Appl. Phys. B **74**, 521 (2002).
20. F. Bai, Q. Wang, Z. Liu, X. Zhang, W. Sun, X. Wan, P. Li, G. Jin, and H. Zhang, Opt. Let. **36**, 813 (2011).
21. A. Sabella, J. A. Piper, and R. P. Mildren, Opt. Let. **39**, 4037 (2014).